ACS Catalysis

pubs.acs.org/acscatalysis Research Article

Mechanistic Insights into CO_2 Electroreduction on Ni_2P: Understanding Its Selectivity toward Multicarbon Products

Sayan Banerjee, Arvin Kakekhani, Robert B. Wexler, and Andrew M. Rappe*

Cite This: *ACS Catal.* 2021, 11, 11706−11715 Read Online

ACCESS | Metrics & More | Article Recommendations | Supporting Information

ABSTRACT: Recently, nickel phosphides (Ni_xP_y) have been reported to enable selective electrochemical formation of multicarbon products (C_3 and C_4) *via* the CO_2 reduction reaction (CO_2RR); nevertheless, their activities remain low. In order to understand the roots of their high selectivity and low activity and to direct the design of more active Ni_xP_y-based CO_2RR catalysts, we investigate the CO_2RR mechanism on Ni_2P using density functional theory (DFT) calculations. We reveal that the reaction proceeds through the formate pathway, followed by formaldehyde (H_2CO^*) formation and self-condensation. Moreover, we demonstrate that surface hydride transfer steps, along with surface-mediated C−C coupling, are essential in order to avoid C_1 product formation and boost selectivity toward multicarbon products. In addition, we find that the thermal surface hydride transfer from the surface to the physisorbed CO_2 is one of the key rate-limiting steps, and since it is not electroactive, it cannot be accelerated by applying an overpotential. Finally, our results also show that the hydrogen affinity of the surface and the dynamic surface reconstruction *via* H adsorption facilitate selective CO_2 reduction and C−C coupling on Ni_2P. These findings provide an impetus for exploring materials design space to identify the physical principles that govern the thermodynamics of rate-limiting thermal steps in electrocatalytic processes.

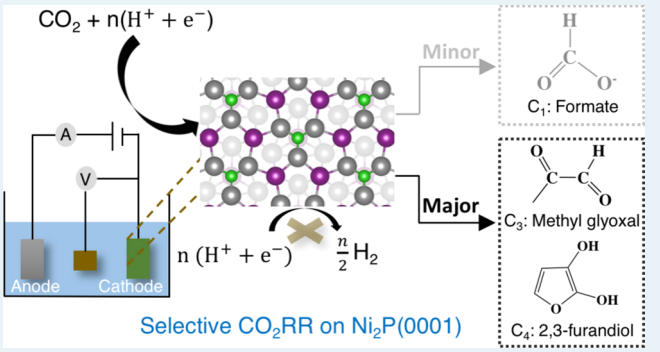

KEYWORDS: *nickel phosphides, CO_2, electroreduction, multicarbon products*

INTRODUCTION

Reducing CO_2 to hydrocarbons and chemical feedstocks (*e.g.*, alcohols, aldehydes, ketones, *etc.*) is a crucial challenge of the 21st century, due to its environmental and industrial consequences.[1,2] Thus, designing active and selective catalysts for the CO_2RR has become a very active area of research. Electrocatalysis, for example, using Cu, transition metal oxides, phosphides, and chalcogenides, has attracted much attention in recent years, as it provides promising avenues for CO_2 reduction.[3−8] However, even the state-of-the-art catalysts for the CO_2RR suffer from activity, selectivity, and stability issues that limit their widespread implementation.[5,9] In particular, the high kinetic barrier associated with CO_2 activation and competition between the CO_2RR and the hydrogen evolution reaction (HER) under reducing conditions are major challenges impeding the simultaneous improvement of the activity and selectivity of CO_2RR catalysts.[5,10,11] Additionally, the application of electrode potentials and the presence of adsorbates has also been shown to induce surface reconstructions,[12−19] thus further complicating the design of electrocatalysts for the CO_2RR.[12,20−24]

Surface reconstruction is a set of phenomena at which the surface stoichiometry and/or atomic configuration change relative to the bulk.[25−27] Such changes occur in order to help the surface cope with the broken bonds resulting from surface formation and to reduce the surface Gibbs free energy.[28] There are numerous examples of this phenomenon, including the formation of oxide monolayers on silver surfaces,[29,30] formation of ultrathin oxide layers on nitrides,[31] surface hydrogenation of phosphides,[12,32] and nonstoichiometric surface reconstruction of polar and ferroelectric materials.[27,33,34] The reconstructed surfaces can have significantly different surface chemistry and catalytic properties than the bulk-like surfaces.[35−37]

To date, Cu is the most widely used catalyst for the CO_2RR, due to its high Faradaic efficiency (FE). However, it does generate a mixture of products, lacking the desired selectivity toward C_1, C_2, and C_3 products (where the subscript corresponds to the number of carbons in a product).[3,7,38−48] Recently, there have been efforts to use chemical treatments to render Cu-based systems more selective toward C_2 product

Received: August 16, 2021

https://doi.org/10.1021/acscatal.1c03639
ACS Catal. 2021, 11, 11706−11715

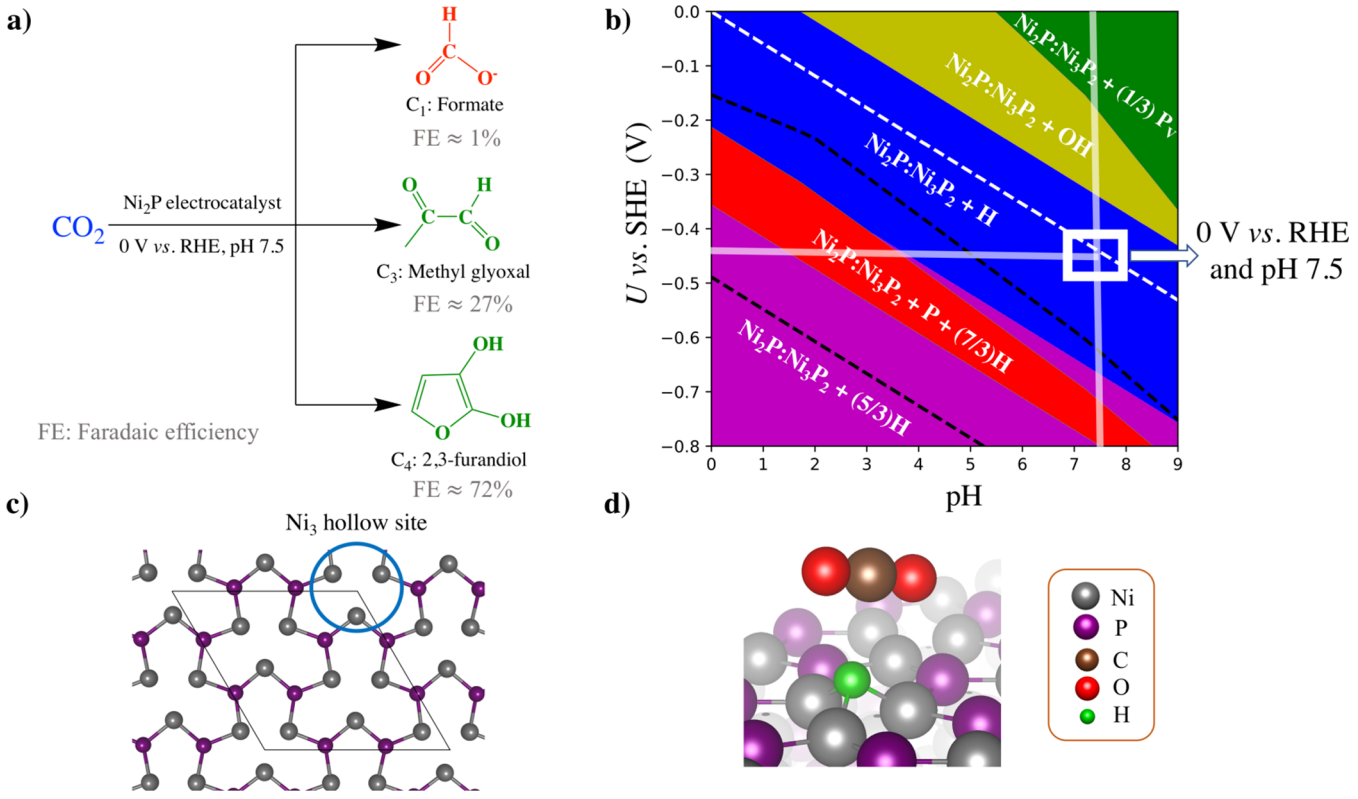

Figure 1. (a) CO_2RR products on Ni_2P, along with the experimental conditions used to perform the reaction.[68] Formate (C_1) is the minor product (shown in red, FE ≈ 1%), whereas methyl glyoxal (C_3, FE ≈ 27%) and 2,3-furandiol (C_4, FE ≈ 72%) are the major products (shown in green). (b) Computed surface phase diagram of $Ni_2P(0001)$ in equilibrium with 1 M H_3PO_4 or 1 M PH_3 and Ni(s) or 1 M Ni^{2+}. The stable surface at 0 V *vs* RHE is Ni_2P/Ni_3P_2 + H (blue shaded region). The white box encloses the experimental *U* and pH conditions. Black dashed lines correspond to the bulk stability region under aqueous conditions and the white dashed line is the HER line.[12] (c) Ni_3P_2 termination of $Ni_2P(0001)$. The Ni_3 hollow site, which is found to strongly bind H ($\Delta G = -0.46$ eV) and the CO_2RR intermediates, is enclosed by a blue circle. (d) CO_2 and H coadsorption geometry on Ni_2P/Ni_3P_2. The color code is Ni (gray), P (purple), C (brown), O (red), and H (green).

formation.[49] In addition to Cu and Cu-based materials, transition-metal oxides and chalcogenides also have been developed as CO_2RR catalysts; however, it remains challenging to attain both high activity and high selectivity for multicarbon product formation using these materials.[23,50−58]

Over the last 20 years, theoretical investigations have provided significant mechanistic insights for overcoming the limitations associated with the CO_2RR. For example, it was shown that the CO_2 activation *via* H transfer from the solvent to either the C (to form formate HCOO*) or one of the O atoms (to form hydrocarboxylate HOCO*) of CO_2 has a large kinetic barrier.[10,59] Therefore, lowering the CO_2 activation barrier is a crucial target for improving the activity of CO_2RR catalysts.[10,59−61] Additionally, it has been proposed that pathways involving the formate intermediate lead primarily to C_1 products, whereas those involving carbon monoxide (CO*) as the key intermediate (formed *via* surface-adsorbed HOCO*) are more likely to generate multicarbon products.[5,40,41,43,52,62−65] In this regard, the electrochemical barrier for CO* to CHO* has been identified as another important descriptor for the selectivity of CO_2RR catalysts toward multicarbon product formation.[5,41,66,67]

Recently, nickel phosphides (Ni_xP_y) were reported to exhibit high selectivity toward multicarbon products possessing the chemically precious keto (C_3) and heterocyclic furan (C_4) moieties (Figure 1a).[68] More specifically, at 0 V versus RHE and pH 7.5, high selectivity was observed toward C_3 (methyl glyoxal, FE ≈ 27%) and C_4 (2,3-furandiol, FE ≈ 72%) products (shown in green); the C_1 (formate, FE ≈ 1%) product was obtained only in small amounts (shown in red).[68] While selectivity toward multicarbon products was achieved, the catalysts suffer from low activity, with multicarbon product yields on the order of micromoles.[68] While previous experimental and theoretical studies have revealed and explained the catalytic activity of Ni_xP_y toward other reactions such as the HER,[12,32,69−72] there are no previous studies that explain their activity and selectivity toward multicarbon product formation *via* the CO_2RR.[68] Hence, detailed mechanistic studies are needed to provide insights into the origin of the high selectivity and low activity of Ni_2P, ultimately leading the way to design improved catalysts for selective multicarbon product formation.

Here, we present mechanistic insights into the remarkably selective formation of valuable multicarbon products *via* the CO_2RR on Ni_2P. First, we identify the thermodynamically stable surface under experimental conditions by including the effect of pH and the electrochemical potential.[12,68] Next, we investigate CO_2 activation, leading to the prediction that the CO_2RR on Ni_2P follows the formate (HCOO*) pathway. We determine that the large barrier for CO_2 activation *via* surface H transfer and formate (HCOO*) to formic acid (HCOOH*) transformation step limits the catalytic activity of Ni_2P and results in the low turnover frequency that was observed experimentally. Next, we explain how the formate pathway leads to the formation of formaldehyde (H_2CO*) which later undergoes C−C coupling. It is shown that the strong hydrogen

https://doi.org/10.1021/acscatal.1c03639
ACS Catal. 2021, 11, 11706−11715

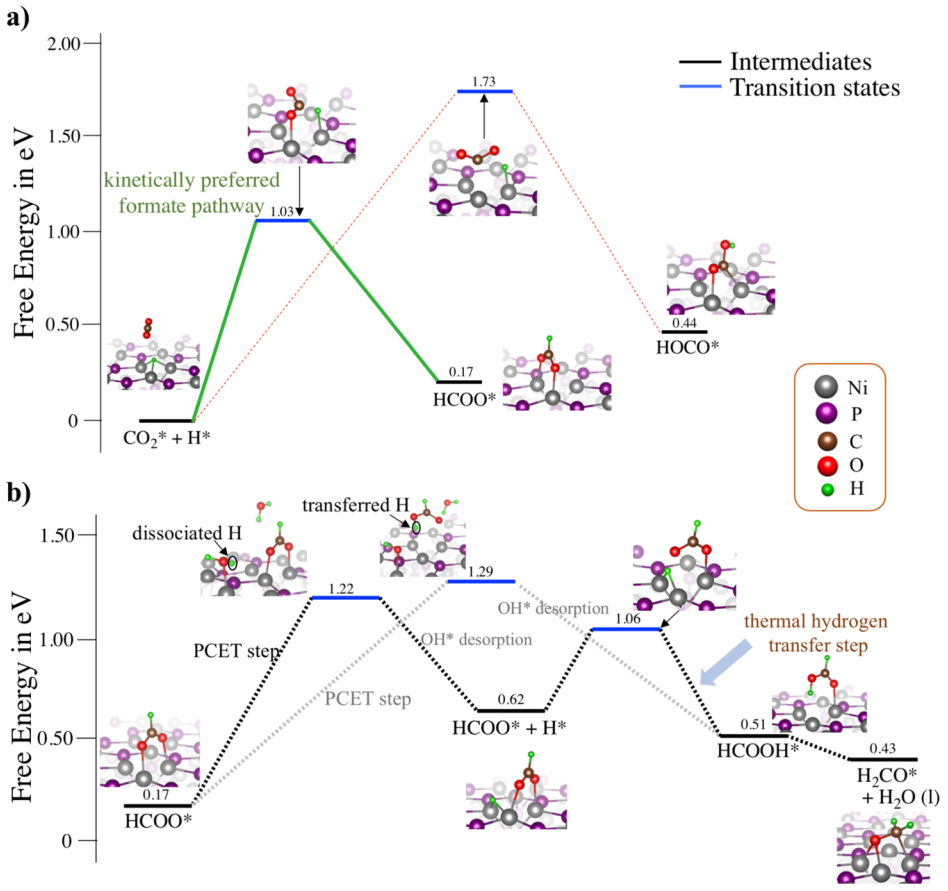

Figure 2. Free-energy diagrams for (a) CO_2 activation and (b) H_2CO^* formation. In (a), we compare the relative energies of the two competing pathways for hydrogen transfer. Green (kinetically favored) and red (kinetically disfavored) lines correspond to the formation of the formate (HCOO*) and hydrocarboxyl (HOCO*) intermediates, respectively. Transition states (blue lines) are shown for both pathways. (b) Formation of H_2CO^* from HCOO*, where insets show the binding geometries for each intermediate. The more favorable pathway is shown in black dashed lines and the less favorable pathway is shown in dashed gray. The color code is Ni (gray), P (purple), C (brown), O (red), and H (green).

affinity of the surface, leading to H* adsorption, drives the intermediates toward the C−C bond formation steps. In particular, we find that the availability of multiple H-binding sites on the surface facilitates H_2CO^* self-condensation. Finally, we describe how a sequence of C−C coupling steps and other important chemical transformations (*e.g.*, enol−keto tautomerization, water elimination, and cyclization) leads to the formation of the experimentally observed C_3 and C_4 products.[68]

METHODS

DFT calculations of the thermodynamics and kinetics of the CO_2RR on Ni_2P were carried out using the Quantum ESPRESSO software package.[73] The electronic exchange−correlation energy was calculated using the generalized gradient approximation of Perdew, Burke, and Ernzerhof (PBE).[10,12,74,75] A kinetic energy cutoff of 50 Ry was used to expand the wave functions of the valence electrons in a plane-wave basis. The OPIUM (version 3.7) software was used to generate designed, optimized, norm-conserving, nonlocal pseudopotentials.[76−78] The DFT-D3 correction developed by Grimme *et al.* was used to capture dispersion interactions, which are crucial to model catalytic transformations.[79−83]

Both experiment and theory identify Ni_3P_2 as the thermodynamically stable termination of $Ni_2P(0001)$ (Figure 1c).[12,84−86] For this reason, we modeled the CO_2RR on the Ni_3P_2-terminated $Ni_2P(0001)$ surface using a periodic slab with eight layers along the *c* lattice vector and 20 Å of vacuum. We use a $(\sqrt{3} \times \sqrt{3})R30°$ surface unit cell instead of the 1 × 1 in order to minimize the interaction between adsorbates in periodic images and to provide ample room for modeling diffusion kinetics. A Γ-centered, 2 × 2 × 1 *k*-point grid was used to sample the Brillouin zone. We used the climbing image nudged elastic band (CI-NEB) method to calculate kinetic barriers for the thermal steps.[87] The computational hydrogen electrode model was used to capture the pH and potential dependence of the free energies of the reaction intermediates.[41]

Surface phase diagrams under realistic aqueous conditions were constructed using the procedure outlined in the literature.[12−14] Similar to a previous work,[12] we find that $Ni_2P(0001)$ adsorbs H* in the Ni_3 hollow site (Figure 1b) under the experimental conditions (0 V vs RHE and pH 7.5). In order to compute the contributions of the zero-point energy and vibrational entropy to the free-energy change for each reaction step, we conducted vibrational frequency analysis within the harmonic approximation (Table S1 in Supporting Information). The kinetic barrier of the proton coupled electron transfer steps is calculated using an explicit solvation approach (with some implicit solvation also performed for benchmarking purposes) and the calculation details are given in Supporting Information.

https://doi.org/10.1021/acscatal.1c03639
ACS Catal. 2021, 11, 11706−11715

RESULTS AND DISCUSSION

CO_2 Activation. Here, we model the activation of CO_2 *via* the formation of either HCOO* or HOCO* at the Ni_3 hollow site on Ni_2P (Ni_3P_2 termination). We find that under the experimental equilibrium conditions, the Ni_3 hollow site is occupied by H* (Figure 1b), consistent with previous theoretical studies.[12,71,88] Since Ni_2P is metallic and H_2O binds weakly to metallic surfaces[89] and the O 2*p* lone pair is repelled by the hydridic nature of H* (physisorption energy of H_2O on H adsorbed Ni_3P_2 termination is −0.26 eV),[12,69,89] there is no significant site competition between H_2O and CO_2. Consequently, the physisorbed CO_2* geometry can be considered as a reasonable geometry for the CO_2RR on Ni_2P, even in the presence of the aqueous environment.[10,41] Specifically, we find that CO_2 physisorbs (with a physisorption energy of −0.16 eV) above the H* at the Ni_3 hollow site (Figure 1d). In this physisorbed geometry, the C of CO_2 is 2.13 Å from the H*, and one of the O atoms is closer to the surface (3.67 Å away from surface) than the other (4.26 Å away from surface).[10] Due to this starting geometry and the preoccupation of the surface active site with a H*, CO_2 activation requires surface H transfer, which does not only activate the CO_2 but empties the active site for the resulting intermediate. Such a reaction is a thermal step (as opposed to electrochemical) and is thus unaffected by changes in the electrode potential. This hydride transfer can occur through two pathways: to the C of physisorbed CO_2 to produce formate (HCOO*) or to one of its O atoms to produce hydrocarboxylate (HOCO*).[5,10,41,52] We find that the ΔG values for the reaction of CO_2* and H* to form HCOO* and HOCO* are 0.16 and 0.44 eV, respectively (difference in free energy between the initial and final states in Figure 2a). Therefore, HCOO* is the thermodynamically preferred intermediate. Additionally, the kinetic barrier associated with HCOO* formation (1.03 eV) is much smaller than that of HOCO* formation (1.73 eV), thus practically eliminating any pathways involving the HOCO* intermediate from consideration. The dual thermodynamic and kinetic preference for CO_2 hydrogenation at the partially positively charged C atom [see the transition state (TS) shown in Figure 2a] is likely related to the hydridic nature of H* at the Ni_3 hollow site.[12] The kinetic barrier for CO_2 activation to HCOO* (1.03 eV) is related to the energy penalties associated with CO_2 bending[10] (see the TS for the green dotted pathway in Figure 2a, noting that the linear physisorbed CO_2 molecule bends upon interaction with H*) and H* migration from the Ni_3 hollow site to a top Ni site.[12] We also note that compared to bare transition-metal surfaces, the electrostatics created by partial positive (Ni) and negative (P and hydridic H*) sites on the surface can help lower the thermal CO_2 activation step by providing some stabilization to the transition state. In summary, we find that the initiation of the CO_2RR on Ni_2P involves HCOO* formation and identify the large kinetic barrier of HCOO* formation (1.03 eV) *via* surface hydride transfer as one of the root causes for the low turnover frequency observed experimentally.[68]

Formation of Formaldehyde from Formate. Following the generation of HCOO*, it can either desorb or participate in further reactions. We investigate two different pathways for further reduction of the adsorbed HCOO*: (a) the first pathway involves a proton-coupled electron transfer (PCET)-assisted rearrangement of HCOO* at the Ni_3 hollow site (forming a so-called "co-adsorbed geometry" with the neighboring H*), followed by a surface hydrogenation step (*via* transfer of the neighboring H*) to form HCOOH*, and (b) the second pathway involves the direct protonation of HCOO* *via* PCET to form HCOOH*. We find that the first pathway *via* formate rearrangement is the energetically preferred one as discussed below. Here, the surface catalyzes the H_2O dissociation event by forming a surface-bound H* at the Ni−Ni bridge site, while the OH* is bound to an adjacent Ni site (see the TS corresponding to the PCET step in the black dashed line in Figure 2b). Compared to bare transition-metal surfaces, the electrostatics of the surface created by surface partial charges helps stabilize the surface−water interactions,[89] thus lowering the corresponding barrier of the surface-mediated PCET step. We have calculated the proton-coupled electron transfer barrier by considering two water molecules. Such an approach is found to be sufficient to understand the reaction energetics in the case of the CO_2RR on RuO_2[90] and the oxygen evolution reaction on RuO_2, IrO_2, and TiO_2.[91] Here, we consider that the PCET happens *via* the H of one of the H_2O and the OH* binds to the surface. The other H_2O can then stabilize such an intermediate. Like the CO_2RR on RuO_2,[90] the desorption barrier of OH* is not calculated, and we assume that OH* is in equilibrium with the bulk solution. Further details for calculating the kinetic barrier of the PCET steps are given in the Section 1.c of Supporting Information.

Regarding the first pathway, the kinetic barrier associated with the formation of the co-adsorbed HCOO* + H* intermediate *via* PCET is found to be 1.05 eV (black dashed line from HCOO* to HCOO* + H* in Figure 2b). Furthermore, the co-adsorbed state of HCOO* and H* is 0.45 eV higher in free energy than HCOO* (at 0 V vs RHE). As a result of such HCOO* rearrangement to a higher energy co-adsorbed (HCOO* + H*) intermediate and the entropic driving force to go beyond a nonzero concentration in solution, a small concentration of formate will build up in the solution, thus explaining why it is a minor product in experiments.[68] Additionally, it is worth mentioning that in this co-adsorbed (HCOO* + H*) geometry, H* is close to (2.30 Å O···H*) the nearest O of HCOO* (HCOO* + H* in Figure 2b), which facilitates the formation of HCOOH* *via* thermal surface hydrogenation. We find that the kinetic barrier for H* transfer to HCOO* is 0.44 eV ("thermal hydrogen transfer step" in Figure 2b) and thus easily surmountable at room temperature.

Regarding the second pathway, we find that the kinetic barrier for the formation of HCOOH* through the direct protonation of HCOO* at one of the O centers is 1.12 eV (shown as a dashed gray line in Figure 2b). Thus, the formation of HCOOH* is energetically more favorable *via* the co-adsorbed (HCOO* + H*) intermediate rather than the PCET-mediated direct protonation of HCOO*.

Once the HCOOH* forms, it undergoes water elimination consisting of two consecutive downhill PCET steps, to form H_2CO* (Figure 2b). We find that surface hydrogen affinity facilitates the HCOO* rearrangement process and subsequently causes HCOO* hydrogenation to form HCOOH*. Therefore, because HCOO* can react with H* and because Ni_2P adsorbs H strongly, the HCOO* that forms can react to form H_2CO* and onward to multicarbon product formation (as shown in the next sections), avoiding surface poisoning. This route, with formate leading to multicarbon products

https://doi.org/10.1021/acscatal.1c03639
ACS Catal. 2021, 11, 11706−11715

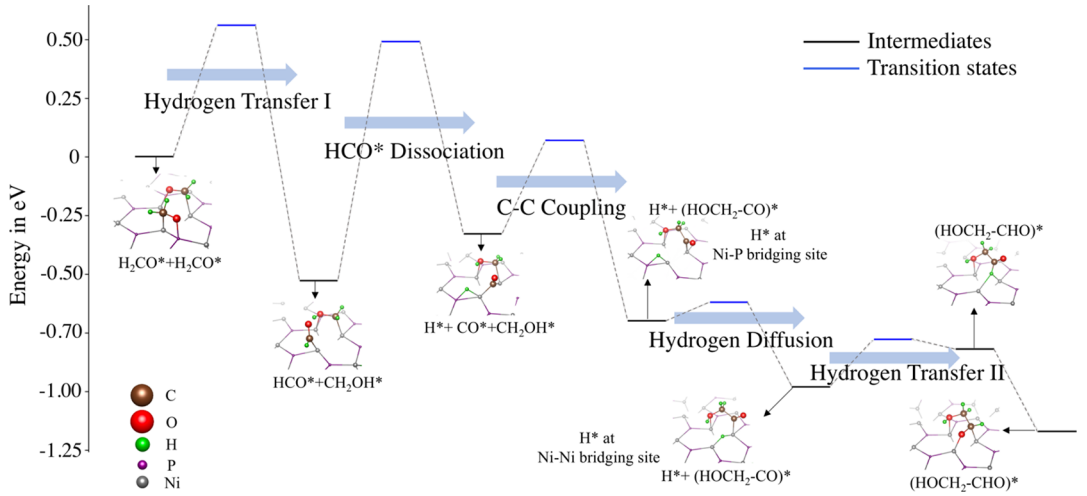

Figure 3. Mechanism for H_2CO^* self-condensation. Binding geometries are shown for each intermediate. The color code is Ni (gray), P (purple), C (brown), O (red), and H (green). The atomic radii of Ni and P are not drawn to scale in order to improve clarity. The energies of the intermediates are relative to that of the first geometry on the left, where two H_2CO^* are close to one another at a Ni_3 hollow site. For the overall energy diagram of the CO_2RR on Ni_2P, see Figures 2b and 4.

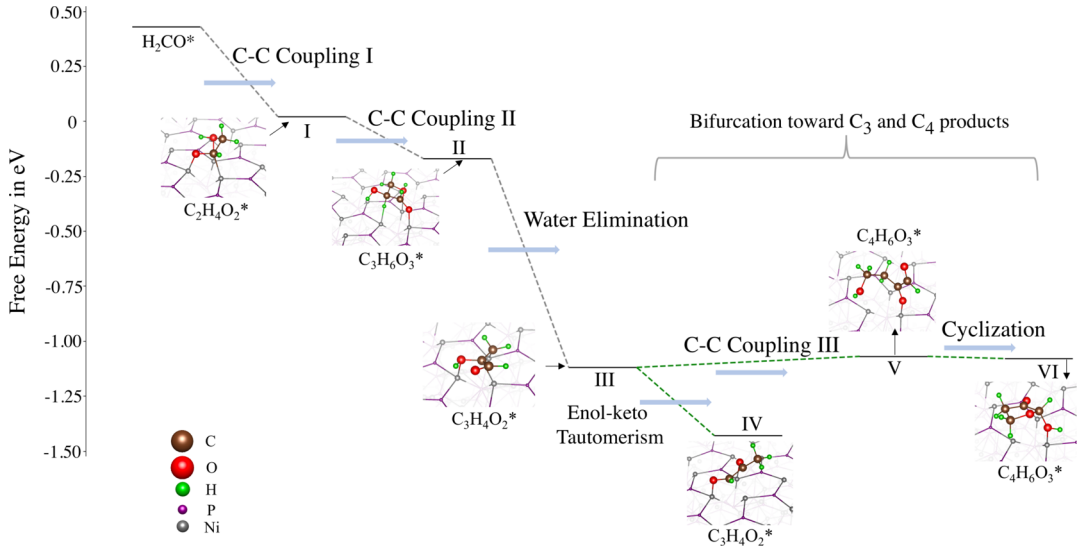

Figure 4. Mechanism for multicarbon product formation *via* the formaldehyde (H_2CO^*) intermediate. Insets show the structures of the surface-bound intermediates. The color code is Ni (gray), P (purple), C (brown), O (red), and H (green). The indices 1−6 correspond to the following intermediates I: glycolaldehyde; II: glyceraldehyde; III: 2-hydroxy-2-propenal; IV: methyl glyoxal; V: 4-hydroxy-2-oxo-butanal; and VI: dihydro-2-hydroxy-furanone.

(shown in the next sections) on Ni_2P is in contrast to the previously proposed CO_2RR mechanisms on other materials (*e.g.*, Cu and RuO_2) where formate has been considered as a dead end.[5,41,52] We also identify that the HCOO* to HCOOH* transformation step, which has a net barrier of 1.05 eV, is also a potential target for future studies to improve the turnover frequency of the CO_2RR catalytic cycle on Ni_2P. The HCOO*-mediated pathway proposed here is also supported by the controlled experiment where formate was used as the reactant instead of CO_2,[68] and the same product distribution was observed when CO_2 was used as the reactant (Figure 1a).

C−C Bond Formation through Formaldehyde Self-Condensation. We investigated the possible branching from H_2CO^* toward different intermediates, for example, CH_3O^* and CH_2OH^*, to understand the pathway toward multicarbon products. We considered the feasibility of the formation of different C_1 products, for example, CH_3OH and CH_4, as a potential competitor to a C−C coupling step which would lead to the multicarbon intermediates and products. We find that the C_1 product formation steps are associated with higher kinetic barriers than the H_2CO^* self-coupling step (see Figure S1 in Supporting Information). We find that H_2CO^* can further reduce to CH_2OH^* which can in principle diffuse and self-condensate; nevertheless, the CH_2OH^* diffusion is associated with a higher kinetic barrier. Hence, we continue to propose that the major self-condensation mechanism responsible for multicarbon product formation is H_2CO^* self-coupling. A detailed discussion involving the thermodynamics and the kinetic barriers of the different possible branches from H_2CO^* is given in Supporting Information (see Section 2 of Supporting Information and Figure S1).

Previously, it has been shown that pathways involving the H_2CO^* intermediate are predisposed to the formation of

https://doi.org/10.1021/acscatal.1c03639
ACS Catal. 2021, 11, 11706−11715

multicarbon products, due to the ease with which H_2CO^* undergoes self-condensation *via* a C−C coupling reaction.[42,92] We find that H_2CO^* diffusion also is assisted by H* replenishment at the Ni_3 hollow site (see Figure S1 and the discussion in the Section 2 of Supporting Information). As shown in Figure S1, H_2CO^* diffusion can prepare two H_2CO^* in a favorable orientation for self-condensation (left-most intermediate in Figure 3).

Next, we investigate the mechanism for H_2CO^* self-condensation which includes four crucial steps. The first step involves H transfer between two adjacent H_2CO^* (kinetic barrier of 0.56 eV), which results in the formation of HCO* and CH_2OH^* (Figure 3, shown as "Hydrogen Transfer I"). In the second step, HCO* dissociates, forming CO* and H* at the Ni−Ni and Ni−P bridging sites, respectively (Figure 3, shown as "HCO* Dissociation"). In the third and key step of H_2CO^* self-condensation, CO* and CH_2OH^* react to form a C−C bond with a modest kinetic barrier of 0.40 eV (Figure 3, shown as "C−C Coupling"). The H* stays at the Ni−P bridging site, until the C−C coupling occurs (Figure 3, shown as "C−C Coupling"); subsequently, it diffuses to the Ni−Ni bridging site (Figure 3, shown as "Hydrogen Diffusion"). At the fourth (final) step, the H* attaches to the keto group of the $(HOCH_2-CO)^*$, producing glycolaldehyde ($(HOCH_2-CHO)^*$) (Figure 3, shown as "Hydrogen Transfer II"). Once all of the bonds in glycoaldehyde are formed, its C−C bond rotates in order for the molecule to acquire a more stable adsorption geometry (last step in Figure 3).

At this point, we would like to emphasize that surface H affinity plays a crucial role in multicarbon product formation by facilitating the C−C coupling step. More specifically, the $Ni_2P(0001)$ surface provides multiple H-binding sites (Ni_3 hollow, Ni top, Ni−Ni, and Ni−P bridging) that, when not occupied by H or other adsorbates, can dehydrogenate intermediates in the CO_2RR, making it possible for two H_2CO^* to undergo C−C coupling while avoiding steric hindrance induced by their C−H groups. As per Figure 4, the C−C coupling *via* H_2CO^* self-condensation is thermodynamically downhill, suggesting that the formation of multicarbon intermediates on Ni_2P is more favorable than the formation of C_1 products (such as formate). Therefore, the PCET-assisted rearrangement of HCOO*, discussed in the previous section and shown in Figure 2b, ultimately leads to a thermodynamically downhill C−C coupling step, further justifying our proposed mechanism thus far.

Toward C_3 and C_4 Products. In this final section, we investigate the pathway from glycolaldehyde to the experimentally observed C_3 and C_4 products.[68] As we have already explained in the preceding section, the first step (to form intermediate I in Figure 4) involves C−C coupling *via* the self-condensation of H_2CO^* to form glycolaldehyde ($(HOCH_2-CHO)^*$), which is thermodynamically downhill by 0.41 eV. For both H_2CO^* and glycolaldehyde, the −C═O moiety is parallel to the surface (similar to H_2CO^*, see the adsorbed H_2CO^* in Figure 2b). This orientation exposes the aldehyde center of glycolaldehyde* and makes it more susceptible to C−C coupling with other H_2CO^* species. The C−C coupling reaction of glycolaldehyde* and H_2CO^* is thermodynamically downhill by 0.19 eV and produces glyceraldehyde* (intermediate II in Figure 4). Next, glyceraldehyde* undergoes water elimination, where either the terminal OH or the OH attached to the central carbon atom takes part in the elimination step. We find that the removal of the terminal OH, which proceeds *via* syn intramolecular water elimination, is 0.30 eV more thermodynamically favorable than the elimination pathway involving the OH attached to the central carbon of glyceraldehyde. Overall, the water elimination step is thermodynamically downhill by 0.96 eV (shown as "Water Elimination" in Figure 4) and results in the formation of 2-hydroxy-2-propenal (intermediate III in Figure 4).

Once 2-hydroxy-2-propenal has formed, there is the possibility of bifurcation in the reaction pathway (shown by green dotted lines in Figure 4). Either the enol compound (III in Figure 4) can undergo enol−keto tautomerization (shown as "Enol−keto Tautomerism" in Figure 4) to form methyl glyoxal (intermediate IV in Figure 4; experimentally observed C_3 product) or it can participate in further C−C coupling (shown as "C−C Coupling III" in Figure 4). The enol-to-keto transformation is downhill by 0.31 eV, whereas the formation of C_4 molecules (intermediates V and VI in Figure 4), *via* C−C coupling and subsequent cyclization, is nearly thermoneutral (Figure 4). In the final step, the cyclic C_4 intermediate (dihydro-2-hydroxy-furanone, intermediate VI in Figure 4) forms 2,3-furandiol (experimentally observed C_4 product, Figure 1a) *via* aromatization. We note that the chemisorption energies of 2,3-furandiol and methyl glyoxal are −0.91 and −1.44 eV (see Table S2 in Supporting Information), respectively. This implies that the desorption of 2,3-furandiol likely is more feasible from a kinetic standpoint, which is in agreement with the experiments by Calvinho *et al.* where more 2,3-furandiol was isolated than methyl glyoxal.[68]

The overall energetics of our proposed mechanism for the CO_2RR on Ni_2P (see Figures 2 and 4) reveals that the formation of multicarbon intermediates (especially C_3 and C_4) *via* PCET-assisted HCOO* rearrangement is strongly exergonic, thus elucidating why C_1 is a minor product, and C_3 and C_4 molecules are the major products.[68] We emphasize that the first hydride transfer in CO_2 activation is one of the key rate-limiting steps, and we propose this as a vital target to improve the catalytic activity in further studies. As the thermal hydride transfer is not amenable to acceleration by overpotential, our results suggest that active site engineering to simultaneously reduce the energy penalty associated with H* migration from the Ni_3 hollow site to the Ni top site[69] and CO_2 bending[61] could potentially reduce the kinetic barrier for hydride transfer. Finally, we propose that the stabilization of the co-adsorbed H*/HCOO* intermediate is another promising strategy to facilitate the transformation of HCOO* to HCOOH*, as this should boost selectivity toward the formation of multicarbon products. To this end, doping and strain could be exploited to reduce the barriers for surface hydride transfers[93] on Ni_2P and optimize the binding of these crucial intermediates.

CONCLUSIONS

We demonstrate that both C_1 (formate) and multicarbon product (methyl glyoxal and 2,3-furandiol) formation proceed through the HCOO* intermediate on Ni_2P. The mechanism proposed here provides an alternative route toward multicarbon product formation, as it predicts a pathway that does not involve a HOCO* intermediate. Such a pathway successfully accounts for the high selectivity (and low activity) toward C_3 and C_4 products, observed in previous experiments.[68] Our results identify the optimization of CO_2* bending and H* migration from Ni_3-hollow to Ni-top site in the CO_2 activation transition state and HCOO* to HCOOH*

https://doi.org/10.1021/acscatal.1c03639
ACS Catal. 2021, 11, 11706−11715

transformation step, as promising targets for improving the catalytic activity. We find that the strong H affinity of the Ni_2P surface and the availability of multiple H-binding sites provide a local reservoir of H* which acts as a reagent source for reduction and hydrogenation of CO_2RR intermediates. Furthermore, surface reconstruction *via* H adsorption in the hollow site creates a thermodynamic driving force for the intermediates such as HCOO* and H_2CO* to proceed toward C−C coupling. We thus propose that the H affinity of the surface can be used as a knob to influence the energetics of the CO_2RR. We find that thermal steps such as surface hydride transfer, surface hydrogenation, diffusion, and self-condensation reactions are integral parts of the electrochemical CO_2 RR on Ni_2P. These findings imply that simultaneous engineering of the thermal and electrochemical steps can open up novel material design strategies for more active CO_2RR catalysts with high selectivity toward multicarbon products.

■ ASSOCIATED CONTENT

Supporting Information

The Supporting Information is available free of charge at https://pubs.acs.org/doi/10.1021/acscatal.1c03639.

Additional computational details, figure showing the competitive pathways for different CO_2RR product formations, tabulated data for free-energy correction, surfaces considered for generating the surface-phase diagram, contribution of the zero-point energy, enthalpic temperature correction, and vibrational entropy to the free energy; possible branching from formaldehyde; plausible branching in the mechanistic pathway from H_2CO*; reaction energy diagram of HCOO* to HCOOH* transformation; chemisorption energies for the multicarbon intermediates; and top and side view of the bare and reconstructed Ni_2P surfaces for Ni_3P_2 termination (PDF)

Structural files for the intermediates and the transition states (ZIP)

■ AUTHOR INFORMATION

Corresponding Author

Andrew M. Rappe − *Department of Chemistry, University of Pennsylvania, Philadelphia, Pennsylvania 19104-6323, United States;* orcid.org/0000-0003-4620-6496; Email: rappe@sas.upenn.edu

Authors

Sayan Banerjee − *Department of Chemistry, University of Pennsylvania, Philadelphia, Pennsylvania 19104-6323, United States;* orcid.org/0000-0002-8586-9236

Arvin Kakekhani − *Department of Chemistry, University of Pennsylvania, Philadelphia, Pennsylvania 19104-6323, United States;* orcid.org/0000-0002-8553-7776

Robert B. Wexler − *Department of Mechanical and Aerospace Engineering, Princeton University, Princeton, New Jersey 08544, United States;* orcid.org/0000-0002-6861-6421

Complete contact information is available at: https://pubs.acs.org/10.1021/acscatal.1c03639

Author Contributions

S.B. performed all the calculations. S.B. and A.K. designed and executed the study with guidance from A.M.R.. R.B.W. helped in understanding the surface structure. S.B., A.K., R.B.W., and A.M.R. wrote the manuscript together.

Notes

The authors declare no competing financial interest.

■ ACKNOWLEDGMENTS

S.B., A.K., R.B.W., and A.M.R.'s work is supported by the Department of Energy, Office of Science, Office of Basic Energy Sciences, under grant number DE-SC0019281. We acknowledge computational support from the National Energy Research Scientific Computing Center.

■ REFERENCES

(1) Lewis, N. S.; Nocera, D. G. Powering the Planet: Chemical Challenges in Solar Energy Utilization. *Proc. Natl. Acad. Sci.* **2006**, *103*, 15729−15735.

(2) Kondratenko, E. V.; Mul, G.; Baltrusaitis, J.; Larrazábal, G. O.; Pérez-Ramírez, J. Status and perspectives of CO2 conversion into fuels and chemicals by catalytic, photocatalytic and electrocatalytic processes. *Energy Environ. Sci.* **2013**, *6*, 3112−3135.

(3) Hori, Y. *Modern Aspects of Electrochemistry*; Vayenas, C. G., White, R. E., Gamboa-Aldeco, M. E., Eds.; Springer: New York, NY, 2008; pp 89−189.

(4) Whipple, D. T.; Kenis, P. J. A. Prospects of CO2 Utilization via Direct Heterogeneous Electrochemical Reduction. *J. Phys. Chem. Lett.* **2010**, *1*, 3451−3458.

(5) Xu, S.; Carter, E. A. Theoretical Insights into Heterogeneous (Photo)electrochemical CO2 Reduction. *Chem. Rev.* **2019**, *119*, 6631−6669.

(6) Gattrell, M.; Gupta, N.; Co, A. A review of the aqueous electrochemical reduction of CO2 to hydrocarbons at copper. *J. Electroanal. Chem.* **2006**, *594*, 1−19.

(7) Nitopi, S.; Bertheussen, E.; Scott, S. B.; Liu, X.; Engstfeld, A. K.; Horch, S.; Seger, B.; Stephens, I. E. L.; Chan, K.; Hahn, C.; Nørskov, J. K.; Jaramillo, T. F.; Chorkendorff, I. Progress and Perspectives of Electrochemical CO2 Reduction on Copper in Aqueous Electrolyte. *Chem. Rev.* **2019**, *119*, 7610−7672 Publisher: American Chemical Society.

(8) Kuhl, K. P.; Hatsukade, T.; Cave, E. R.; Abram, D. N.; Kibsgaard, J.; Jaramillo, T. F. Electrocatalytic Conversion of Carbon Dioxide to Methane and Methanol on Transition Metal Surfaces. *J. Am. Chem. Soc.* **2014**, *136*, 14107−14113 Publisher: American Chemical Society.

(9) Sebastián-Pascual, P.; Mezzavilla, S.; Stephens, I. E. L.; Escudero-Escribano, M. Structure-Sensitivity and Electrolyte Effects in CO_2 Electroreduction: From Model Studies to Applications. *ChemCatChem* **2019**, *11*, 3626−3645 Publisher: John Wiley & Sons, Ltd.

(10) Cheng, T.; Xiao, H.; Goddard, W. A. Reaction Mechanisms for the Electrochemical Reduction of CO2 to CO and Formate on the Cu(100) Surface at 298 K from Quantum Mechanics Free Energy Calculations with Explicit Water. *J. Am. Chem. Soc.* **2016**, *138*, 13802−13805.

(11) Singh, A. R.; Rohr, B. A.; Schwalbe, J. A.; Cargnello, M.; Chan, K.; Jaramillo, T. F.; Chorkendorff, I.; Nørskov, J. K. Electrochemical Ammonia Synthesis-The Selectivity Challenge. *ACS Catal.* **2017**, *7*, 706−709.

(12) Wexler, R. B.; Martirez, J. M. P.; Rappe, A. M. Active Role of Phosphorus in the Hydrogen Evolving Activity of Nickel Phosphide (0001) Surfaces. *ACS Catal.* **2017**, *7*, 7718−7725.

(13) Qiu, T.; Tu, B.; Saldana-Greco, D.; Rappe, A. M. Ab Initio Simulation Explains the Enhancement of Catalytic Oxygen Evolution on CaMnO3. *ACS Catal.* **2018**, *8*, 2218−2224.

(14) Rong, X.; Kolpak, A. M. Ab Initio Approach for Prediction of Oxide Surface Structure, Stoichiometry, and Electrocatalytic Activity in Aqueous Solution. *J. Phys. Chem. Lett.* **2015**, *6*, 1785−1789.

(15) Reuter, K.; Scheffler, M. Composition and structure of the RuO_2(110) surface in an O_2 and CO environment: Implications for

the catalytic formation ofCO2. *Phys. Rev. B: Condens. Matter Mater. Phys.* **2003**, *68*, 045407 Publisher: American Physical Society.
(16) Gong, X.-Q.; Selloni, A.; Vittadini, A. Density Functional Theory Study of Formic Acid Adsorption on Anatase TiO2(001): Geometries, Energetics, and Effects of Coverage, Hydration, and Reconstruction. *J. Phys. Chem. B* **2006**, *110*, 2804−2811 Publisher: American Chemical Society.
(17) Deshlahra, P.; Conway, J.; Wolf, E. E.; Schneider, W. F. Influence of Dipole-Dipole Interactions on Coverage-Dependent Adsorption: CO and NO on Pt(111). *Langmuir* **2012**, *28*, 8408−8417 Publisher: American Chemical Society.
(18) Frey, K.; Schmidt, D. J.; Wolverton, C.; Schneider, W. F. Implications of Coverage-dependent O Adsorption for Catalytic NO Oxidation on the late Transition Metals. *Catal. Sci. Technol.* **2014**, *4*, 4356−4365 Publisher: The Royal Society of Chemistry.
(19) Deshlahra, P.; Schneider, W. F.; Bernstein, G. H.; Wolf, E. E. Direct Control of Electron Transfer to the Surface-CO Bond on a Pt/TiO2 Catalytic Diode. *J. Am. Chem. Soc.* **2011**, *133*, 16459−16467 Publisher: American Chemical Society.
(20) Gunathunge, C. M.; Li, X.; Li, J.; Hicks, R. P.; Ovalle, V. J.; Waegele, M. M. Spectroscopic Observation of Reversible Surface Reconstruction of Copper Electrodes under CO2 Reduction. *J. Phys. Chem. C* **2017**, *121*, 12337−12344.
(21) Eren, B.; Zherebetskyy, D.; Patera, L. L.; Wu, C. H.; Bluhm, H.; Africh, C.; Wang, L.-W.; Somorjai, G. A.; Salmeron, M. Activation of Cu(111) Surface by Decomposition into Nanoclusters driven by CO Adsorption. *Science* **2016**, *351*, 475−478.
(22) Kim, Y.-G.; Baricuatro, J. H.; Javier, A.; Gregoire, J. M.; Soriaga, M. P. The Evolution of the Polycrystalline Copper Surface, First to Cu(111) and Then to Cu(100), at a Fixed CO2RR Potential: A Study by Operando EC-STM. *Langmuir* **2014**, *30*, 15053−15056.
(23) Le, M.; Ren, M.; Zhang, Z.; Sprunger, P. T.; Kurtz, R. L.; Flake, J. C. Electrochemical Reduction of CO2 to CH3OH at Copper Oxide Surfaces. *J. Electrochem. Soc.* **2011**, *158*, E45−E49.
(24) Cho, M.; Song, J. T.; Back, S.; Jung, Y.; Oh, J. The Role of Adsorbed CN and Cl on an Au Electrode for Electrochemical CO2 Reduction. *ACS Catal.* **2018**, *8*, 1178−1185 Publisher: American Chemical Society.
(25) Cook, S.; Marks, L. D. Ab Initio Predictions of Double-Layer TiO2-Terminated SrTiO3(001) Surface Reconstructions. *J. Phys. Chem. C* **2018**, *122*, 21991−21997 Publisher: American Chemical Society.
(26) Di Valentin, C.; Pacchioni, G.; Selloni, A. Electronic Structure of Defect States in Hydroxylated and Reduced RutileTiO2(110)-Surfaces. *Phys. Rev. Lett.* **2006**, *97*, 166803 Publisher: American Physical Society.
(27) Martirez, J. M. P.; Morales, E. H.; Saidi, W. A.; Bonnell, D. A.; Rappe, A. M. Atomic and Electronic Structure of theBaTiO3(001)(5×5)R26.6°Surface Reconstruction. *Phys. Rev. Lett.* **2012**, *109*, 256802 Publisher: American Physical Society.
(28) Rogal, J.; Reuter, K.; Scheffler, M. Thermodynamic Stability of PdO Surfaces. *Phys. Rev. B: Condens. Matter Mater. Phys.* **2004**, *69*, 075421 Publisher: American Physical Society.
(29) Wexler, R. B.; Qiu, T.; Rappe, A. M. Automatic Prediction of Surface Phase Diagrams Using Ab Initio Grand Canonical Monte Carlo. *J. Phys. Chem. C* **2019**, *123*, 2321−2328 Publisher: American Chemical Society.
(30) Li, W.-X.; Stampfl, C.; Scheffler, M. Subsurface Oxygen and Surface Oxide formation at Ag(111): A Density-functional Theory Investigation. *Phys. Rev. B: Condens. Matter Mater. Phys.* **2003**, *67*, 045408 Publisher: American Physical Society.
(31) Abroshan, H.; Bothra, P.; Back, S.; Kulkarni, A.; Nørskov, J. K.; Siahrostami, S. Ultrathin Cobalt Oxide Overlayer Promotes Catalytic Activity of Cobalt Nitride for the Oxygen Reduction Reaction. *J. Phys. Chem. C* **2018**, *122*, 4783−4791 Publisher: American Chemical Society.
(32) Laursen, A. B.; Wexler, R. B.; Whitaker, M. J.; Izett, E. J.; Calvinho, K. U. D.; Hwang, S.; Rucker, R.; Wang, H.; Li, J.; Garfunkel, E.; Greenblatt, M.; Rappe, A. M.; Dismukes, G. C. Climbing the Volcano of Electrocatalytic Activity while Avoiding Catalyst Corrosion: Ni3P, a Hydrogen Evolution Electrocatalyst Stable in Both Acid and Alkali. *ACS Catal.* **2018**, *8*, 4408−4419.
(33) Garrity, K.; Kakekhani, A.; Kolpak, A.; Ismail-Beigi, S. Ferroelectric Surface Chemistry: First-principles Study of the $PbTiO_3$ Surface. *Phys. Rev. B: Condens. Matter Mater. Phys.* **2013**, *88*, 045401 Publisher: American Physical Society.
(34) Rasmussen, M. K.; Foster, A. S.; Hinnemann, B.; Canova, F. F.; Helveg, S.; Meinander, K.; Martin, N. M.; Knudsen, J.; Vlad, A.; Lundgren, E.; Stierle, A.; Besenbacher, F.; Lauritsen, J. V. Stable cation inversion at the MgAl2O4(100) surface. *Phys. Rev. Lett.* **2011**, *107*, 036102 Publisher: American Physical Society.
(35) Martirez, J. M. P.; Kim, S.; Morales, E. H.; Diroll, B. T.; Cargnello, M.; Gordon, T. R.; Murray, C. B.; Bonnell, D. A.; Rappe, A. M. Synergistic Oxygen Evolving Activity of a TiO2-Rich Reconstructed SrTiO3(001) Surface. *J. Am. Chem. Soc.* **2015**, *137*, 2939−2947 Publisher: American Chemical Society.
(36) Polo-Garzon, F.; Fung, V.; Liu, X.; Hood, Z. D.; Bickel, E. E.; Bai, L.; Tian, H.; Foo, G. S.; Chi, M.; Jiang, D.-e.; Wu, Z. Understanding the Impact of Surface Reconstruction of Perovskite Catalysts on CH4 Activation and Combustion. *ACS Catal.* **2018**, *8*, 10306−10315 Publisher: American Chemical Society.
(37) Li, Y.-F.; Aschauer, U.; Chen, J.; Selloni, A. Adsorption and Reactions of O2 on Anatase TiO2. *Acc. Chem. Res.* **2014**, *47*, 3361−3368 Publisher: American Chemical Society.
(38) Tang, W.; Peterson, A. A.; Varela, A. S.; Jovanov, Z. P.; Bech, L.; Durand, W. J.; Dahl, S.; Nørskov, J. K.; Chorkendorff, I. The importance of surface morphology in controlling the selectivity of polycrystalline copper for CO2 electroreduction. *Phys. Chem. Chem. Phys.* **2012**, *14*, 76−81.
(39) Kuhl, K. P.; Cave, E. R.; Abram, D. N.; Jaramillo, T. F. New insights into the electrochemical reduction of carbon dioxide on metallic copper surfaces. *Energy Environ. Sci.* **2012**, *5*, 7050−7059.
(40) Garza, A. J.; Bell, A. T.; Head-Gordon, M. Mechanism of CO2 Reduction at Copper Surfaces: Pathways to C2 Products. *ACS Catal.* **2018**, *8*, 1490−1499.
(41) Peterson, A. A.; Abild-Pedersen, F.; Studt, F.; Rossmeisl, J.; Nørskov, J. K. How Copper Catalyzes the Electroreduction of Carbon Dioxide into Hydrocarbon Fuels. *Energy Environ. Sci.* **2010**, *3*, 1311−1315.
(42) Montoya, J. H.; Peterson, A. A.; Nørskov, J. K. Insights into C−C Coupling in CO2Electroreduction on Copper Electrodes. *ChemCatChem* **2013**, *5*, 737−742.
(43) Calle-Vallejo, F.; Koper, M. T. M. Theoretical Considerations on the Electroreduction of CO to C2Species on Cu(100) Electrodes. *Angew. Chem., Int. Ed.* **2013**, *52*, 7282−7285.
(44) Schreier, M.; Héroguel, F.; Steier, L.; Ahmad, S.; Luterbacher, J. S.; Mayer, M. T.; Luo, J.; Grätzel, M. Solar Conversion of CO_2 to CO using Earth-abundant Electrocatalysts Prepared by Atomic Layer Modification of CuO. *Nat. Energy* **2017**, *2*, 17087 Number: 7 Publisher: Nature Publishing Group.
(45) Ma, M.; Djanashvili, K.; Smith, W. A. Selective electrochemical reduction of CO2to CO on CuO-derived Cu nanowires. *Phys. Chem. Chem. Phys.* **2015**, *17*, 20861−20867 Publisher: Royal Society of Chemistry.
(46) Ma, M.; Djanashvili, K.; Smith, W. A. Controllable Hydrocarbon Formation from the Electrochemical Reduction of CO2 over Cu Nanowire Arrays. *Angew. Chem., Int. Ed.* **2016**, *55*, 6680−6684.
(47) De Gregorio, G. L.; Burdyny, T.; Loiudice, A.; Iyengar, P.; Smith, W. A.; Buonsanti, R. Facet-Dependent Selectivity of Cu Catalysts in Electrochemical CO2 Reduction at Commercially Viable Current Densities. *ACS Catal.* **2020**, *10*, 4854−4862 Publisher: American Chemical Society.
(48) Loiudice, A.; Lobaccaro, P.; Kamali, E. A.; Thao, T.; Huang, B. H.; Ager, J. W.; Buonsanti, R. Tailoring Copper Nanocrystals towards C 2 Products in Electrochemical CO 2 Reduction. *Angew. Chem., Int. Ed.* **2016**, *55*, 5789−5792.
(49) Ma, W.; Xie, S.; Liu, T.; Fan, Q.; Ye, J.; Sun, F.; Jiang, Z.; Zhang, Q.; Cheng, J.; Wang, Y. Electrocatalytic Reduction of CO_2 to

https://doi.org/10.1021/acscatal.1c03639
ACS Catal. 2021, 11, 11706−11715

Ethylene and Ethanol through Hydrogen-assisted C−C Coupling over Fluorine-modified Copper. *Nat. Catal.* **2020**, *3*, 478 Publisher: Nature Publishing Group.
(50) Qu, J.; Zhang, X.; Wang, Y.; Xie, C. Electrochemical reduction of CO2 on RuO2/TiO2 nanotubes composite modified Pt electrode. *Electrochim. Acta* **2005**, *50*, 3576−3580.
(51) Spataru, N.; Tokuhiro, K.; Terashima, C.; Rao, T. N.; Fujishima, A. Electrochemical Reduction of Carbon Dioxide at Ruthenium Dioxide Deposited on Boron-doped Diamond. *J. Appl. Electrochem.* **2003**, *33*, 1205−1210.
(52) Karamad, M.; Hansen, H. A.; Rossmeisl, J.; Nørskov, J. K. Mechanistic Pathway in the Electrochemical Reduction of CO2 on RuO2. *ACS Catal.* **2015**, *5*, 4075−4081.
(53) Mezzavilla, S.; Katayama, Y.; Rao, R.; Hwang, J.; Regoutz, A.; Shao-Horn, Y.; Chorkendorff, I.; Stephens, I. E. L. Activity-or Lack Thereof-of RuO2-Based Electrodes in the Electrocatalytic Reduction of CO2. *J. Phys. Chem. C* **2019**, *123*, 17765−17773 Publisher: American Chemical Society.
(54) Asadi, M.; Kim, K.; Liu, C.; Addepalli, A. V.; Abbasi, P.; Yasaei, P.; Phillips, P.; Behranginia, A.; Cerrato, J. M.; Haasch, R.; Zapol, P.; Kumar, B.; Klie, R. F.; Abiade, J.; Curtiss, L. A.; Salehi-Khojin, A. Nanostructured transition metal dichalcogenide electrocatalysts for CO 2 reduction in ionic liquid. *Science* **2016**, *353*, 467−470 Publisher: American Association for the Advancement of Science Section: Report.
(55) Asadi, M.; Kumar, B.; Behranginia, A.; Rosen, B. A.; Baskin, A.; Repnin, N.; Pisasale, D.; Phillips, P.; Zhu, W.; Haasch, R.; Klie, R. F.; Král, P.; Abiade, J.; Salehi-Khojin, A. Robust Carbon Dioxide Reduction on Molybdenum Disulphide Edges. *Nat. Commun.* **2014**, *5*, 4470 Number: 1 Publisher: Nature Publishing Group.
(56) Chan, K.; Tsai, C.; Hansen, H. A.; Nørskov, J. K. Molybdenum Sulfides and Selenides as Possible Electrocatalysts for CO2Reduction. *ChemCatChem* **2014**, *6*, 1899−1905 Publisher: John Wiley & Sons, Ltd.
(57) Duyar, M. S.; Tsai, C.; Snider, J. L.; Singh, J. A.; Gallo, A.; Yoo, J. S.; Medford, A. J.; Abild-Pedersen, F.; Studt, F.; Kibsgaard, J.; Bent, S. F.; Nørskov, J. K.; Jaramillo, T. F. A Highly Active Molybdenum Phosphide Catalyst for Methanol Synthesis from CO and CO 2. *Angew. Chem., Int. Ed.* **2018**, *57*, 15045−15050.
(58) Janke, C.; Duyar, M. S.; Hoskins, M.; Farrauto, R. Catalytic and adsorption studies for the hydrogenation of CO2 to methane. *Appl. Catal., B* **2014**, *152*−*153*, 184−191.
(59) Zhao, X.; Liu, Y. Unveiling the Active Structure of Single Nickel Atom Catalysis: Critical Roles of Charge Capacity and Hydrogen Bonding. *J. Am. Chem. Soc.* **2020**, *142*, 5773−5777 Publisher: American Chemical Society.
(60) Hossain, M. D.; Huang, Y.; Yu, T. H.; Goddard III, W. A., Iii; Luo, Z. Reaction mechanism and kinetics for CO2 reduction on nickel single atom catalysts from quantum mechanics. *Nat. Commun.* **2020**, *11*, 2256 Number: 1 Publisher: Nature Publishing Group.
(61) Zhou, B.; Ou, P.; Pant, N.; Cheng, S.; Vanka, S.; Chu, S.; Rashid, R. T.; Botton, G.; Song, J.; Mi, Z. Highly efficient binary copper−iron catalyst for photoelectrochemical carbon dioxide reduction toward methane. *Proc. Natl. Acad. Sci.* **2020**, *117*, 1330−1338.
(62) Cheng, T.; Xiao, H.; Goddard, W. A. Full Atomistic Reaction Mechanism with Kinetics for CO Reduction on Cu(100) from ab initio Molecular Dynamics Free-energy Calculations at 298 K. *Proc. Natl. Acad. Sci.* **2017**, *114*, 1795−1800 Publisher: National Academy of Sciences Section: Physical Sciences.
(63) Xiao, H.; Goddard, W. A.; Cheng, T.; Liu, Y. Cu metal embedded in oxidized matrix catalyst to promote CO2 activation and CO dimerization for electrochemical reduction of CO2. *Proc. Natl. Acad. Sci.* **2017**, *114*, 6685−6688 Publisher: National Academy of Sciences Section: Physical Sciences.
(64) Back, S.; Kim, J.-H.; Kim, Y.-T.; Jung, Y. On the mechanism of high product selectivity for HCOOH using Pb in CO2 electroreduction. *Phys. Chem. Chem. Phys.* **2016**, *18*, 9652−9657 Publisher: Royal Society of Chemistry.
(65) Back, S.; Kim, H.; Jung, Y. Selective Heterogeneous CO2 Electroreduction to Methanol. *ACS Catal.* **2015**, *5*, 965−971 Publisher: American Chemical Society.
(66) Peterson, A. A.; Nørskov, J. K. Activity Descriptors for CO2 Electroreduction to Methane on Transition-Metal Catalysts. *J. Phys. Chem. Lett.* **2012**, *3*, 251−258 Publisher: American Chemical Society.
(67) Pérez-Gallent, E.; Figueiredo, M. C.; Calle-Vallejo, F.; Koper, M. T. M. Spectroscopic Observation of a Hydrogenated CO Dimer Intermediate During CO Reduction on Cu(100) Electrodes. *Angew. Chem., Int. Ed.* **2017**, *56*, 3621−3624.
(68) Calvinho, K. U. D.; Laursen, A. B.; Yap, K. M. K.; Goetjen, T. A.; Hwang, S.; Murali, N.; Mejia-Sosa, B.; Lubarski, A.; Teeluck, K. M.; Hall, E. S.; Garfunkel, E.; Greenblatt, M.; Dismukes, G. C. Selective CO2 reduction to C3 and C4 oxyhydrocarbons on nickel phosphides at overpotentials as low as 10 mV. *Energy Environ. Sci.* **2018**, *11*, 2550−2559.
(69) Wexler, R. B.; Martirez, J. M. P.; Rappe, A. M. Chemical Pressure-Driven Enhancement of the Hydrogen Evolving Activity of Ni2P from Nonmetal Surface Doping Interpreted via Machine Learning. *J. Am. Chem. Soc.* **2018**, *140*, 4678−4683.
(70) Popczun, E. J.; McKone, J. R.; Read, C. G.; Biacchi, A. J.; Wiltrout, A. M.; Lewis, N. S.; Schaak, R. E. Nanostructured Nickel Phosphide as an Electrocatalyst for the Hydrogen Evolution Reaction. *J. Am. Chem. Soc.* **2013**, *135*, 9267−9270.
(71) Liu, P.; Rodriguez, J. A. Catalysts for Hydrogen Evolution from the [NiFe] Hydrogenase to the Ni2P(001) Surface: The Importance of Ensemble Effect. *J. Am. Chem. Soc.* **2005**, *127*, 14871−14878.
(72) Liu, T.; Li, A.; Wang, C.; Zhou, W.; Liu, S.; Guo, L. Interfacial Electron Transfer of Ni2 P-NiP2 Polymorphs Inducing Enhanced Electrochemical Properties. *Adv. Mater.* **2018**, *30*, 1803590.
(73) Giannozzi, P.; Baroni, S.; Bonini, N.; Calandra, M.; Car, R.; Cavazzoni, C.; Ceresoli, D.; Chiarotti, G. L.; Cococcioni, M.; Dabo, I.; Dal Corso, A.; de Gironcoli, S.; Fabris, S.; Fratesi, G.; Gebauer, R.; Gerstmann, U.; Gougoussis, C.; Kokalj, A.; Lazzeri, M.; Martin-Samos, L.; Marzari, N.; Mauri, F.; Mazzarello, R.; Paolini, S.; Pasquarello, A.; Paulatto, L.; Sbraccia, C.; Scandolo, S.; Sclauzero, G.; Seitsonen, A. P.; Smogunov, A.; Umari, P.; Wentzcovitch, R. M. QUANTUM ESPRESSO: A Modular and Open-source Software Project for Quantum Simulations of Materials. *J. Phys.: Condens. Matter* **2009**, *21*, 395502.
(74) Perdew, J. P.; Burke, K.; Ernzerhof, M. Generalized Gradient Approximation Made Simple. *Phys. Rev. Lett.* **1996**, *77*, 3865−3868.
(75) Nie, X.; Esopi, M. R.; Janik, M. J.; Asthagiri, A. Selectivity of CO2Reduction on Copper Electrodes: The Role of the Kinetics of Elementary Steps. *Angew. Chem., Int. Ed.* **2013**, *52*, 2459−2462.
(76) Rappe, A. M.; Rabe, K. M.; Kaxiras, E.; Joannopoulos, J. D. Optimized Pseudopotentials. *Phys. Rev. B: Condens. Matter Mater. Phys.* **1990**, *41*, 1227−1230.
(77) Ramer, N. J.; Rappe, A. M. Designed Nonlocal Pseudopotentials for Enhanced Transferability. *Phys. Rev. B: Condens. Matter Mater. Phys.* **1999**, *59*, 12471−12478.
(78) Opium: Pseudopotential Generation Project. http://opium.sourceforge.net/ (accessed Aug 16, 2007).
(79) Grimme, S.; Antony, J.; Ehrlich, S.; Krieg, H. A Consistent and Accurate ab initio Parametrization of Density Functional Dispersion Correction (DFT-D) for the 94 Elements H-Pu. *J. Chem. Phys.* **2010**, *132*, 154104.
(80) Moellmann, J.; Grimme, S. DFT-D3 Study of Some Molecular Crystals. *J. Phys. Chem. C* **2014**, *118*, 7615−7621 Publisher: American Chemical Society.
(81) Hujo, W.; Grimme, S. Comparison of the Performance of Dispersion-Corrected Density Functional Theory for Weak Hydrogen Bonds. *Phys. Chem. Chem. Phys.* **2011**, *13*, 13942−13950 Publisher: The Royal Society of Chemistry.
(82) Ramalho, J. P. P.; Gomes, J. R. B.; Illas, F. Accounting for van der Waals Interactions between Adsorbates and Surfaces in Density Functional Theory based Calculations: Selected Examples. *RSC Adv.* **2013**, *3*, 13085−13100 Publisher: The Royal Society of Chemistry.

https://doi.org/10.1021/acscatal.1c03639
ACS Catal. 2021, 11, 11706−11715

(83) Davis, J. B. A.; Baletto, F.; Johnston, R. L. The Effect of Dispersion Correction on the Adsorption of CO on Metallic Nanoparticles. *J. Phys. Chem. A* **2015**, *119*, 9703−9709 Publisher: American Chemical Society.
(84) Wexler, R. B.; Martirez, J. M. P.; Rappe, A. M. Stable Phosphorus-Enriched (0001) Surfaces of Nickel Phosphides. *Chem. Mater.* **2016**, *28*, 5365−5372.
(85) Suzuki, S.; Moula, G. M.; Miyamoto, T.; Nakagawa, Y.; Kinosthita, K.; Asakura, K.; Oyama, S. T.; Otani, S. Scanning Tunneling Microscopy and Photoemission Electron Microscopy Studies on Single Crystal Ni2P Surfaces. *J. Nanosci. Nanotechnol.* **2009**, *9*, 195−201.
(86) Hernandez, A. B.; Ariga, H.; Takakusagi, S.; Kinoshita, K.; Suzuki, S.; Otani, S.; Oyama, S. T.; Asakura, K. Dynamical LEED analysis of Ni2P (0001)-1×1: Evidence for P-covered surface structure. *Chem. Phys. Lett.* **2011**, *513*, 48−52.
(87) Henkelman, G.; Uberuaga, B. P.; Jónsson, H. A Climbing Image Nudged Elastic Band Method for Finding Saddle Points and Minimum Energy Paths. *J. Chem. Phys.* **2000**, *113*, 9901−9904.
(88) Kibsgaard, J.; Tsai, C.; Chan, K.; Benck, J. D.; Nørskov, J. K.; Abild-Pedersen, F.; Jaramillo, T. F. Designing an Improved Transition Metal Phosphide Catalyst for Hydrogen Evolution using Experimental and Theoretical Trends. *Energy Environ. Sci.* **2015**, *8*, 3022−3029 Publisher: The Royal Society of Chemistry.
(89) Kakekhani, A.; Roling, L. T.; Kulkarni, A.; Latimer, A. A.; Abroshan, H.; Schumann, J.; AlJama, H.; Siahrostami, S.; Ismail-Beigi, S.; Abild-Pedersen, F.; Nørskov, J. K. Nature of Lone-Pair-Surface Bonds and Their Scaling Relations. *Inorg. Chem.* **2018**, *57*, 7222−7238.
(90) Tayyebi, E.; Hussain, J.; Skúlason, E. Why do RuO2 electrodes catalyze electrochemical CO2 reduction to methanol rather than methane or perhaps neither of those? *Chem. Sci.* **2020**, *11*, 9542−9553 Publisher: The Royal Society of Chemistry.
(91) Siahrostami, S.; Vojvodic, A. Influence of Adsorbed Water on the Oxygen Evolution Reaction on Oxides. *J. Phys. Chem. C* **2015**, *119*, 1032−1037 Publisher: American Chemical Society.
(92) Thripati, S.; Ramabhadran, R. O. Metal-Ion- and Hydrogen-Bond-Mediated Interstellar Prebiotic Chemistry: The First Step in the Formose Reaction. *J. Phys. Chem. A* **2017**, *121*, 8659−8674.
(93) Xu, S.; Carter, E. A. Balancing Competing Reactions in Hydride Transfer Catalysis via Catalyst Surface Doping: The Ionization Energy Descriptor. *J. Am. Chem. Soc.* **2019**, *141*, 9895−9901 Publisher: American Chemical Society.

https://doi.org/10.1021/acscatal.1c03639
ACS Catal. 2021, 11, 11706−11715